REPORT DOCUMENTATION PAGE

Form Approved
OMB No. 0704-0188

1. REPORT DATE *(DD-MM-YYYY)*	2. REPORT TYPE	3. DATES COVERED *(From - To)*
27-11-2020	Final Performance Report	15 Aug 2016 - 31 Dec 2020

4. TITLE AND SUBTITLE
Distributed System Level Thermal Management of High Transient Heat Loads using Microchannel Evaporators

5a. CONTRACT NUMBER

5b. GRANT NUMBER
N00014-16-1-2690

5c. PROGRAM ELEMENT NUMBER

6. AUTHOR(S)
Wen, John T.
Narayanan, Shankar

5d. PROJECT NUMBER

5e. TASK NUMBER

5f. WORK UNIT NUMBER

7. PERFORMING ORGANIZATION NAME(S) AND ADDRESS(ES)
Rensselaer Polytechnic Institute, 110 8th St., Troy, NY 12180-3522

8. PERFORMING ORGANIZATION REPORT NUMBER

9. SPONSORING/MONITORING AGENCY NAME(S) AND ADDRESS(ES)
Office of Naval Research
875 N. Randolph Street Suite 1425 Arlington VA 22203-1995

10. SPONSOR/MONITOR'S ACRONYM(S)
ONR

11. SPONSOR/MONITOR'S REPORT NUMBER(S)

12. DISTRIBUTION/AVAILABILITY STATEMENT
Approved for public release: distribution unlimited.

13. SUPPLEMENTARY NOTES

14. ABSTRACT
This project has conducted simulation and experimental study of microchannel cooling systems, with an emphasis on the mitigation of flow instabilities and the dynamic control of the system performance in the presence of transient heat loads. Results from this project has enhanced our ability to handle multiple evaporators experiencing asynchronous transient heat loads.

15. SUBJECT TERMS
microchannel evaporator, flow instability, two-phase heat transfer, pressure drop oscillation, maldistribution instability, flow synchronization, thermal management

16. SECURITY CLASSIFICATION OF:			17. LIMITATION OF ABSTRACT	18. NUMBER OF PAGES	19a. NAME OF RESPONSIBLE PERSON
a. REPORT	b. ABSTRACT	c. THIS PAGE			John Wen
U	U	U	UU	25	19b. TELEPHONE NUMBER *(Include area code)* 518-441-0470

FINAL PERFORMANCE REPORT

Award Number	**N00014-16-1-2690**
Title of Research	**Distributed System Level Thermal Management of High Transient Heat Loads using Microchannel Evaporators**
Principal Investigators	John T. Wen, Shankar Narayanan
Organization	Rensselaer Polytechnic Institute
Sponsoring Agency	Office of Naval Research
Period of Performance	8/15/2016-12/31/2020

Major Goals

Phase-change in microchannel evaporators can dissipate significantly higher heat fluxes than conventional evaporators. However, microchannel evaporators are prone to flow instabilities such as pressure drop oscillation and flow maldistribution, which can fail the cooling system. Prior studies to understand flow instabilities have been limited to simple open systems, which has limited scope since microchannel evaporators in real applications are part of a closed cycle, and the cooling demands can vary drastically. Hence, the overall goal of this project is to gain a fundamental understanding of the flow instabilities in closed cycles and develop a control strategy to leverage microchannel evaporators.

Accomplished

This project focuses on the analysis of pressure drop oscillation and flow maldistribution occurring in microchannel-integrated vapor compression and pumped liquid cycles. Both systems consist of a condenser, expansion valve, accumulator and a compressor or pump for circulating the refrigerant. Analysis has been conducted using both computational modeling and experiments. The computational analysis uses a combination of lumped dynamic and static models for the individual components to predict the occurrence of flow instabilities for a given operating condition. The experimentally validated models are then used to investigate the role of various system parameters in the overall cooling performance. For both vapor compression and pumped liquid cycles, fluid flow and heat transfer was characterized via experiments and computational modeling. The effect of various system parameters on stability has also been investigated. In both cycles, pressure drop oscillations were observed under certain combinations of system parameters. Our study indicates that varying the expansion valve is effective in suppressing flow oscillations in most cases. On the other hand, an increase in the evaporator heat load would make the oscillations worse.

The fundamental insight gained on the operation of vapor compression and pumped liquid cycles allowed the development of control strategies for suppressing flow instabilities. Several system controllable parameters were utilized to enable a stable operating condition. These parameters include the expansion valve setting, the compressor or pump speed, and the accumulator heat load. Both feed-forward and feed-back controllers were compared to identify a suitable controller design for the closed systems. The dynamically-controlled microchannel-integrated systems were shown to avoid flow instability in the presence of large transient heat loads. Furthermore, the evaporator could be maintained at the required temperature while maximizing the system-level efficiency. We were then able to extend our control methodology for single-evaporator systems to handle multiple-evaporator systems experiencing asynchronous heat loads.

This project has also analyzed flow maldistribution accompanying pressure drop oscillation using computational modeling and experiments. The model predictions indicate that the extent of thermal and flow coupling between parallel channels of a microchannel evaporator can affect flow maldistribution. If the evaporator design, material and system operating conditions are chosen wisely, the thermal and flow coupling can be enhanced and the uneven distribution of flow and heat transfer in different channels can be minimized. Experiments

conducted using different evaporators were then able to demonstrate synchronization of channel performance when the coupling between the channels was improved in the presence of pressure drop oscillation.

Technical Section

1 Introduction

Microchannel cooling involving flow boiling has the potential to be lightweight and compact, dissipate high heat fluxes, and maintain relatively uniform and low temperatures in the presence of dynamic heat loads [1], which are all essential in naval applications. However, flow boiling in microchannels is prone to instabilities, which includes pressure drop oscillation and flow maldistribution in the evaporator channels [2–8]. These instabilities can result in structural vibration and fatigue, leading to the failure of the cooling mechanism [9], which can severely impede the performance of marine applications.

Pressure drop oscillation is a dynamic instability mechanism, which originate from the growing bubbles resulting from evaporation of the refrigerant in the evaporator. Repeated bubble growth in the upstream and downstream directions and rupture are known to cause the flow oscillations [9, 10]. Flow maldistribution across parallel channels is an instability that is known to occur with pressure drop oscillation since multiple flow rates can coexist for the same pressure drop. These instability mechanisms can lead to dry out and low thermal performance [11]. A widely-used passive technique to suppress flow instabilities involves the addition of inlet restrictors and re-entrant cavities in the microchannels [12–16]. However, this approach can increase the pressure drop and pumping power requirements of the cooling system, making it inefficient. Further, the approach does not address the challenge posed by dynamic heat loads. In general, prior experimental studies have focused mainly on the influence of few system parameters on the flow instabilities. Numerical studies have mainly focused on open systems by considering heat transfer to the evaporator and a surge tank to simulate the effect of compressibility in the system [14,17–19]. With the lack of comprehensive studies involving closed systems, it was not clear how system components, like the accumulator, compressor, and valves, affect the flow characteristics and the performance of the cooling system.

This project has conducted a holistic study of microchannel cooling systems, with an emphasis on the mitigation of flow instabilities and the dynamic control of the system performance in the presence of transient heat loads. Results from this project has enhanced our ability to handle multiple evaporators experiencing asynchronous transient heat loads. The main accomplishments of this project and the corresponding journal publications are listed below:

1. The development of generalized computational models to predict the transient performance of microchannel systems, which include pumped liquid and vapor compression cycles, under different operating conditions [20, 21].

2. The development of dynamic control strategies to mitigate pressure drop instability, maximize the heat transfer performance and system efficiency, and handle transient

heat loads successfully [22].

3. The development of modeling and control strategies to synchronize temperature and flow in an averaged sense for heat exchangers with multiple parallel microchannels [23, 24].

4. The development of estimation and control strategies for unanticipated heat loads [25].

2 Computational Modeling of Fluid Flow and Heat Transfer

In general, both finite element and lumped modeling approaches have been utilized in the analysis and performance optimization [3, 9, 20, 26, 27] of microchannel cooling systems. The finite element models show better accuracy in the prediction of system performance, while the spatially-lumped dynamic models are computationally efficient and beneficial for developing control designs. Additionally, since microchannel evaporators are often operated with subcooled liquid at the inlet and two-phase flow at the outlet, a region of the evaporator is occupied by the liquid phase only, while the rest occupied by both liquid and vapor phases (Fig. 1). This distribution of phases in the evaporator is often analyzed as a two-zone lumped model, although some numerical studies have neglected the contribution of the single-phase region to analyze the evaporator as a one-zone lumped model. In order to quantify the error in the prediction of the flow and heat transfer using the lumped-models, we compared it with the corresponding finite element model.

Fig. 1(a) shows the one-zone evaporator model with the two-phase flow at inlet and outlet. Fig. 1(b) shows the two-zone evaporator model with single-phase at the inlet and two-phase flow at the outlet. In both models, the inlet mass flow rate $\dot{m}_i$, inlet density ρ_i and exit pressure P_o are held fixed, and a uniform heat flux $q^{"}$ is applied to the evaporator. In the simulation, we consider a forty-two channel evaporator with the following dimensions for both fluid channels and walls: Width $\times$ Depth $\times$ Length $=$ 250 μm $\times$ 500 μm $\times$ 21.2 mm, as shown in Fig. 1(c). In this case, R134a is used as the refrigerant.

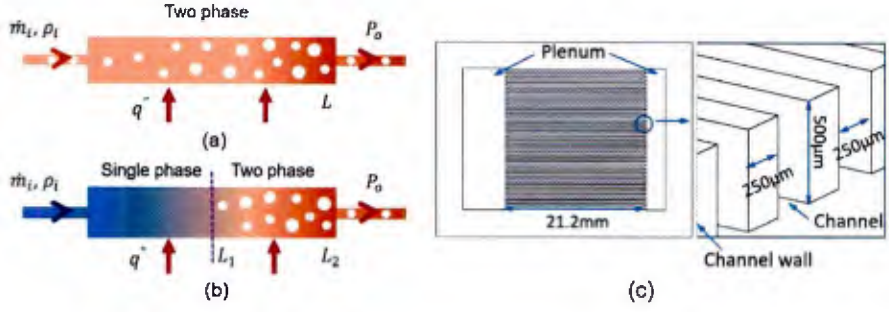

Figure 1: (a) One-zone evaporator model; (b) Two-zone evaporator model; (c) Evaporator design

2.1 Lumped One-zone Model vs. Finite Element Analysis

Fig. 2 shows the prediction of the evaporator performance using the finite element model. Along the evaporator length, the pressure decreases, which corresponds to a lower saturation temperature. Hence, even with evaporator heating, the wall temperature decreases along the evaporator length due to the decrease in the refrigerant temperature. The two-phase heat transfer coefficient (Fig. 2(e)) and pressure gradient (Fig. 2(f)) increase with the vapor quality (Fig. 2(d)), and an increase in the evaporator heat load generally causes a rise in the overall pressure drop and the wall temperature.

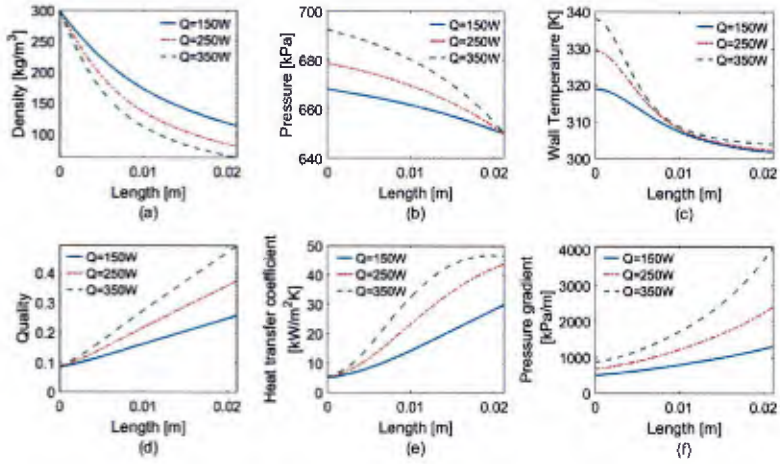

Figure 2: Spatial distributions of (a) density; (b) pressure; (c) wall temperature; (d) quality; (e) heat transfer coefficient; (f) pressure gradient for one-zone finite element model at different heat loads

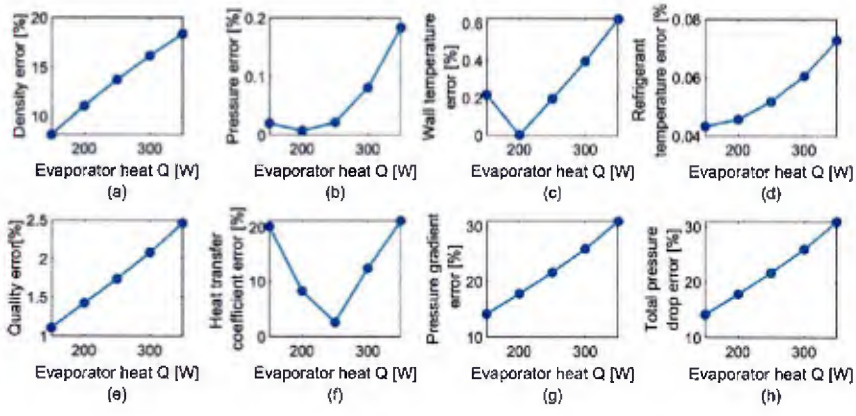

Figure 3: Errors of (a) density; (b) pressure; (c) wall temperature; (d) refrigerant temperature; (e) quality; (f) heat transfer coefficient; (g) pressure gradient; (h) pressure drop for one-zone lumped model at different heat loads

The non-linearity of the heat transfer coefficient and the pressure gradient is expected to affect the accuracy of the lumped one-zone models, especially at higher heat loads. In

this regard, Fig. 3 quantifies the error in the prediction of the lumped model relative to the line-averaged values of the corresponding parameters obtained from the finite element model for different evaporator heat loads. Flow parameters such as refrigerant density, heat transfer coefficient, and pressure drop are highly nonlinear and sensitive to the heat load. In general, we found the errors from the lumped model to increase with heat loads due to higher non-linearity at larger vapor qualities. In summary, the lumped model is more accurate for smaller pressure drops and heat loads (or lower vapor qualities).

2.2 Lumped Two-zone Model vs. Finite Element Analysis

Fig. 4 shows the predicted flow parameters along the length of the evaporator using the finite element model. The dots in the figures indicate the location of saturated liquid where vapor

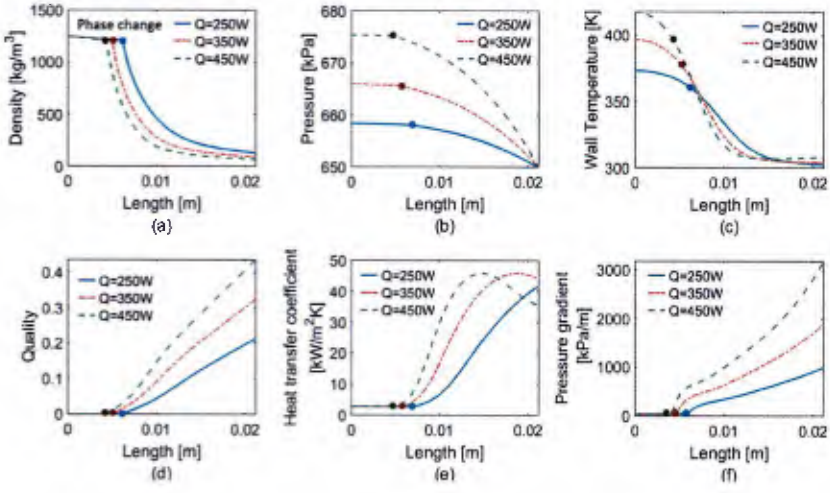

Figure 4: Spatial distributions of (a) density; (b) pressure; (c) wall temperature; (d) quality; (e) heat transfer coefficient; (f) pressure drop gradient of two-zone finite element model at different heat loads

quality is zero. As the heat load increases, the single-phase region shrinks in size. The model indicates that the changes in the flow parameters in the single-phase region are less drastic than the two-phase region of the evaporator due to smaller pressure drops and less sensitivity of fluid properties to the changes in the pressure and temperature. In the two-phase region of the evaporator, the pressure and density profiles show larger non-linearity, which becomes more severe at higher heat loads. Fig. 5 shows the error in the flow predictions using the lumped model relative to the corresponding finite element model at various heat loads. In general, when the exit quality is less than 0.5, the errors in the prediction of the pressure drop and wall temperature are within 15%.

3 Performance Prediction and Dynamic Control

Fig. 6(a) shows the vapor compression cycle (VCC) considered in this project. The cycle operates by compressing saturated refrigerant (R134a) vapor from the accumulator to a

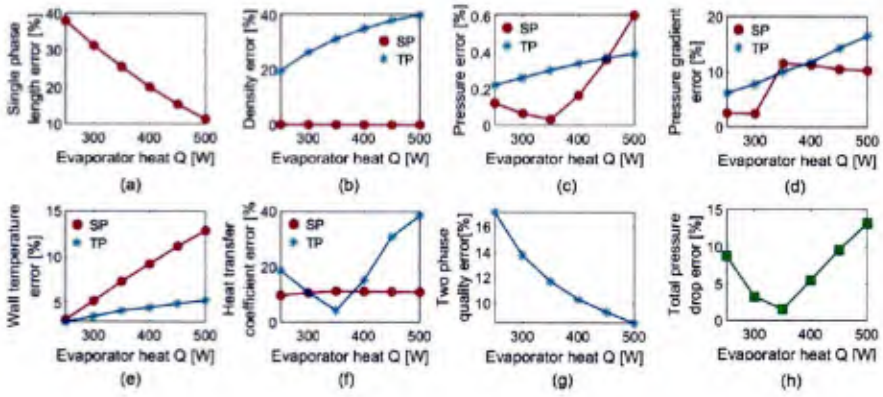

Figure 5: Single-phase (SP) and two-phase (TP) errors of (a) Single-phase length; (b) Density; (c) Pressure; (d) Pressure gradient; (e) Wall temperature; (f) Heat transfer coefficient; (g) Two-phase quality; (h) Total pressure drop for two-zone lumped model at different heat loads

higher pressure and temperature using the compressor. The refrigerant then flows through the condenser to dissipate heat to an external coolant maintained at room temperature. After exiting the condenser as liquid at room temperature, the refrigerant flows through an

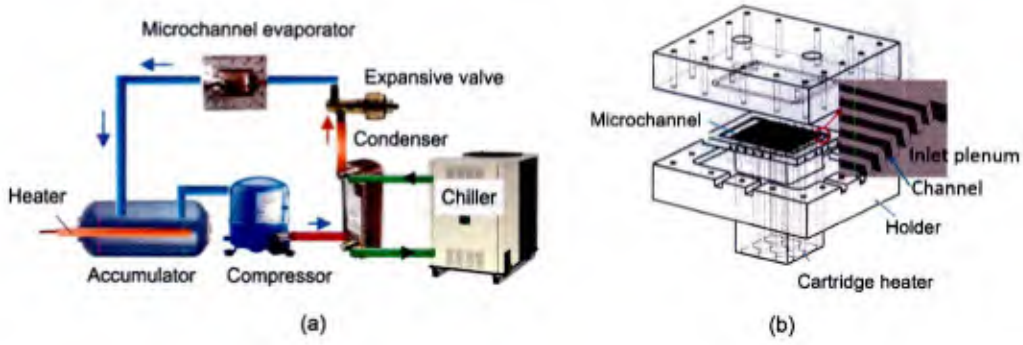

Figure 6: (a) Schematic diagram of the VCC system; (b) Design of microchannel evaporator

electronic expansion valve to exit at low pressure and temperature. The refrigerant then enters the evaporator to absorb heat. The refrigerant exits the evaporator as liquid-vapor mixture, which enters the accumulator to close the refrigeration cycle. The evaporator used in this project has forty-two microchannels with the following dimensions for both fluid channels and walls: Width $\times$ Depth $\times$ Length $=$ 250 μm $\times$ 500 μm $\times$ 21.2 mm, as shown in Fig 6(b). For this system, the controllable parameters are the valve opening (A_v from 5 to 100 %), the accumulator heat load (Q_a from 0 to 800 W) and compressor speed (ω from 20 to 70 Hz). The evaporator heat load is a system disturbance, which can vary from 0 to 900 W.

In this study, the microchannel pressure drop, ΔP_M obtained from experiments, is provided as a third order polynomial function of the refrigerant flow rate and evaporator heat

load, as shown in Fig. 7(a). The heat transfer coefficient, H_e, is interpolated based on experimental data [28], as shown in Fig. 7(b), where H_e is given as a function of the evaporator heat load, Q_e and the exit quality, x_{eo}.

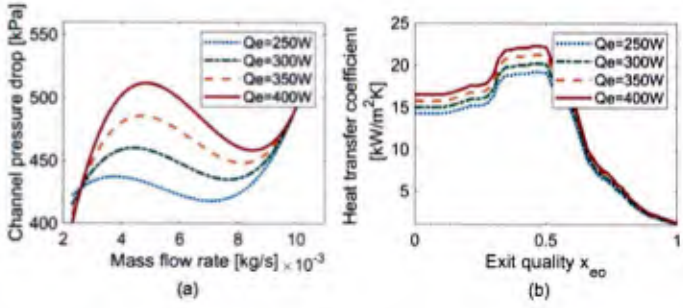

Figure 7: (a) Channel pressure drop vs evaporator mass flow rate and heat load (b) Heat transfer coefficient vs evaporator exit quality and heat load

3.1 Dynamic Control of the VCC Operation

In order to design a controller, optimum operating conditions are first determined using the spatially-lumped two-zone computational model. Optimum operating conditions correspond to those system parameters that provide stable operation, satisfy the required evaporator wall temperature, avoid the critical heat flux and maximize the system-level COP. Using the optimum operating conditions, feedback controller can be designed using MatLab's control system toolbox. Although it is possible to use any system parameter (e.g., temperature, pressure, mass flow rate) as the control output, we use the evaporator wall temperature, T_{we}, since it is usually the parameter of interest for thermal management of electronics.

For the VCC used in this project, the optimum operating condition when Q_e =250 W is A_v =10 %, ω =6 Hz, and Q_a =370 W. As Q_e increases from 250 to 300 to 400 W, the system becomes unstable, and the evaporator wall temperature can potentially exceed the safe operational range (Fig. 8(b)). In this case, a gain-scheduling controller design can be used, which involves selecting the suitable optimum operating conditions and controller parameters based on the evaporator heat load [29]. To demonstrate gain scheduling, we use feedforward control for A_v and feedback control for ω and Q_a. Fig. 8(c) shows the system response to significant changes in Q_e. Hence, gain-scheduling control design avoids flow instability while maintaining the wall temperatures at the desired values, and operating the system around the optimum conditions despite large changes in Q_e.

4 Dynamic Control of Multi-evaporator Cooling System

The understanding gained from performance control of single-evaporator systems was extended to the control of the cooling performance of two-evaporator systems. In this case, we considered a pumped liquid cycle consisting of a pump, a condenser, and two valves

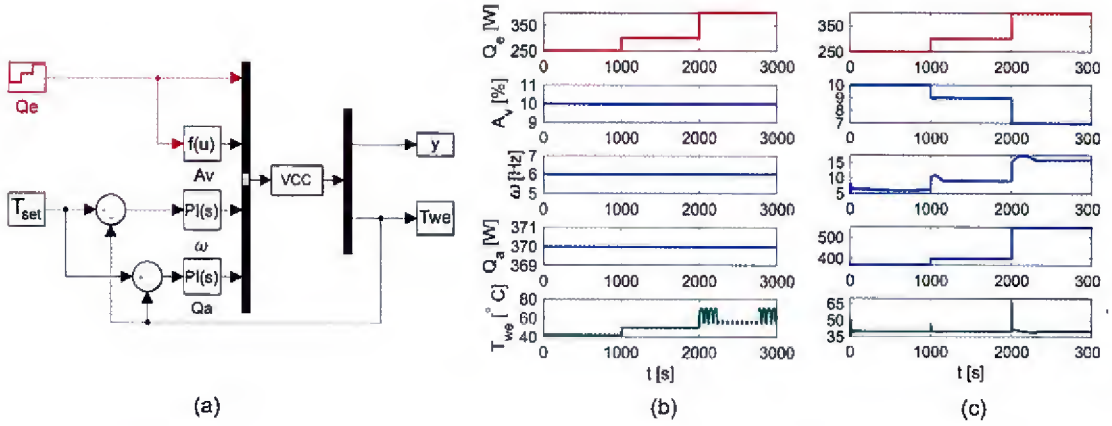

Figure 8: (a) Control diagram; (b) System response without controller; (c) System response with controllers

apart from the evaporators (Fig. 9). Following a procedure similar to the vapor compression cycle, we analyzed the system performance of a pumped liquid cycle under different conditions and heat loads. Optimum operating conditions were then selected to obtain the desired evaporator temperatures, flow conditions to avoid the critical heat flux (CHF), high system efficiency, and robust control. Subsequently, feedforward and feedback controls were designed to ensure system operation close to the chosen optimum conditions, even in the presence of unsynchronized transient heat loads.

4.1 Physical System

Fig. 9(a) illustrates the pumped liquid cycle analyzed in this study. In this system, subcooled refrigerant (R134a), pumped from the condenser, enters the flow control valves at high pressure. The refrigerant streams exit the valves at low pressure to enter the evaporators. As the refrigerant flows through the evaporators, it absorbs heat and exits as a liquid-vapor mixture. Then the refrigerant enters the condenser to release heat to an external coolant maintained at a fixed low temperature. This study considers an evaporator which has fifty-three channels with the following dimensions for fluid channels: Width × Depth × Length = 231 μm × 713 μm × 25.3 mm, and a wall thickness between channels of 231 μm, as illustrated in Fig. 9(b).

For two-phase region, experimental data [4] is used to obtain the average pressure gradient, as shown in Fig. 10(a). The two-phase heat transfer coefficient, H_{tp} based on experimental data [4], is interpolated as a function of the evaporator head flux, q''_e, and the evaporator exit quality, x_{eo}, as shown in Fig. 10(b). The control strategy to maintain uniform evaporator temperatures considers $x_{crit} = 0.45$ as the critical exit quality to ensure safe operation.

4.2 Dynamic Control of the Two-Evaporator System

For different evaporator heat loads, the computational model generates a system operation map for various combinations of the pump speed (ω) and the valve settings (A_{v1}, A_{v2}). The

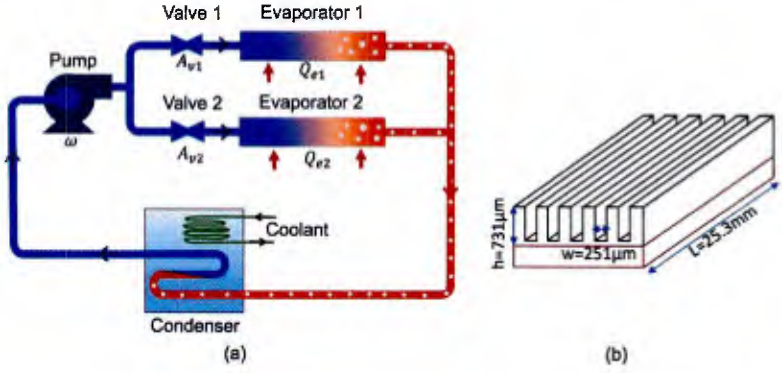

Figure 9: (a) Schematic diagram of the pumped liquid cycle; (b) Evaporator design

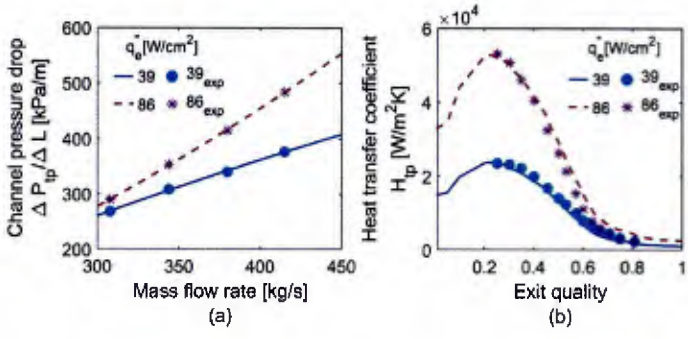

Figure 10: (a) Channel pressure gradient vs. evaporator mass flow rate (b) Heat transfer coefficient vs. evaporator exit quality

selection of optimum operating conditions involves choosing the pump speed (ω) to achieve the desired evaporator temperatures, high COP, and an exit vapor quality to avoid the CHF. Also, the valve settings are chosen to ensure high efficiency and robust control of COP in the presence of transient heat loads. Dynamic control of the system operation is enabled by linearizing the system around the optimum operating conditions for various heat fluxes and tuning the control parameters to obtain the required response time and control robustness.

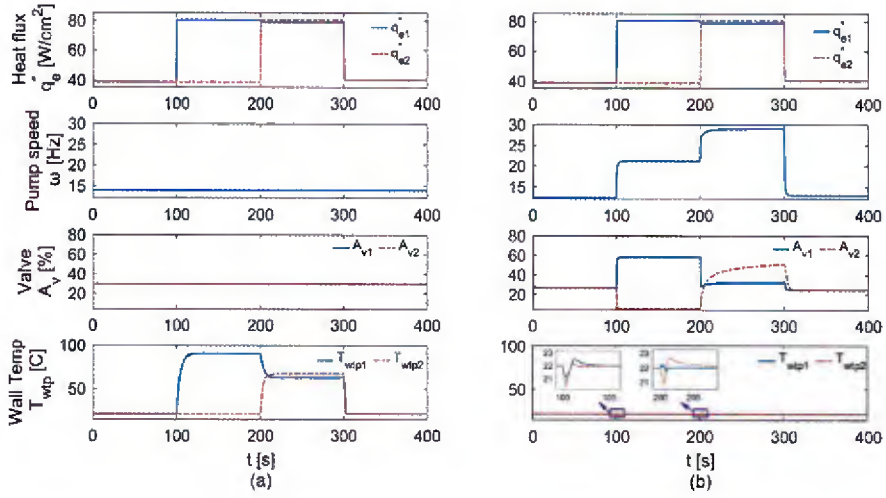

Figure 11: (a) System response without a controller; (b) System response with the controllers

Fig. 11(a) shows the system response without the use of a controller for large variations in the evaporator heat fluxes. With the evaporators experiencing dissimilar heat fluxes, the resulting wall temperatures are significantly different. In addition, the evaporator temperatures can be undesirably high with exit qualities exceeding the critical value ($x_{crit} = 0.45$). This poses a significant risk of dryout and failure of the cooling mechanism. Fig. 11(b) shows the system response using a PI (proportional-integral) control for valve settings A_{v1} and A_{v2}, and the pump speed ω. In this case, active control maintains the wall temperatures at the desired value even when the two evaporators are experiencing significantly different transient heat fluxes.

5 Demonstration of Performance Control and Model Validation

5.1 Performance of a Vapor Compression Cycle

Fig. 12 shows the experimental test-bed of the VCC system used in this project with refrigerant R134a. A cartridge heater is inserted in the accumulator to supply heat to the refrigerant directly which is wired to a BK Precision 1902 DC power supply with a maximum heating power of 900 W. A Danfoss Maneurop MTZ 18-3 reciprocating compressor with a nominal cooling capacity of 2904 W is used in this testbed. A SER-AA electronic expansion valve is controlled with an Intelligent Motion Systems IM483 stepper motor driver.

The condenser is a C-4AG brazed-plate heat exchanger with the coolant pumped using a CFT-150 chiller [29,30]. Using the test-bed described above, we first tested a microchannel

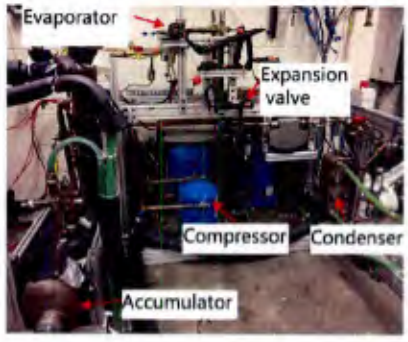

Figure 12: Vapor compression cycle test bed

evaporator with forty-two channels, with the following dimensions for both fluid channels and walls: Width × Depth × Length = 250 μm × 500 μm × 21.2 mm. For the range of operating conditions supported by this test-bed, pressure drop oscillation was not observed. Fig. 13 shows the characterization of the channel pressure drop and heat transfer coefficient for different heat loads. Clearly, our results indicate the absence of a negative slope region in the characterization of pressure drop. We found this to be a practical limitation of the current setup, which prevented the use of lower mass flow rates to observe flow oscillations.

With the use of a different evaporator with relatively larger dimensions, we were able

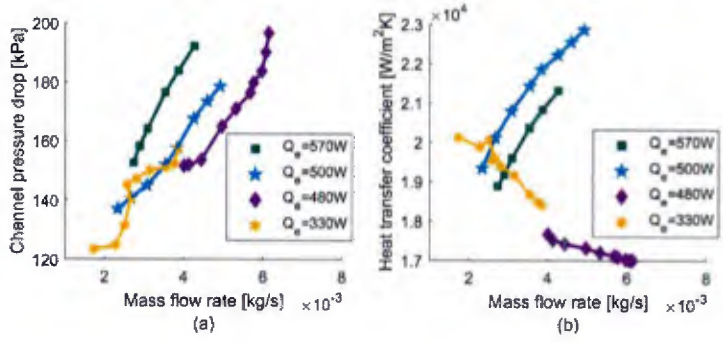

Figure 13: (a) Channel pressure drop; (b) Heat transfer coefficient

to demonstrate pressure drop oscillation. In this design, the evaporator consisted of seven channels with the following dimensions for both fluid channels and walls: Width × Depth × Length = 1 mm ×1 mm ×10 mm. Fig. 14 shows the system stability map obtained experimentally for different accumulator heat loads and valve settings when the evaporator heat load was 130 W. In general, although we found a smaller valve opening to suppress oscillation, under some conditions this may not occur. For instance, when Q_a =150 W, oscillation occurs when the valve opening decreases from 90 % to 80 %. The oscillation takes place due to the reduction of mass flow rate and the characteristic pressure drop consisting of a negative slope region. This phenomenon was also observed in the pumped liquid cycle experiments, as shown later.

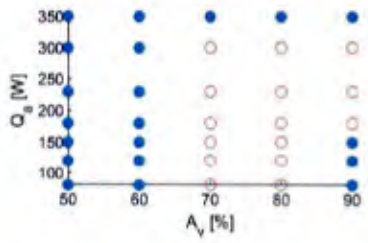

Figure 14: System stability under various combination of valve settings and accumulator heat load at $Q_e = 130$ W (Solid dot: Stable; Hollowed dot: Unstable)

Stability maps, like Fig. 14, can be generated under different evaporator heat load Q_e, which could serve as the guideline to develop a control strategy. For example, Fig. 15 shows the system response for different heat loads with and without the use of a controller. In this case, the experiments demonstrate our capability to address variations in the evaporator heat load and avoiding the pressure drop oscillation by using feedforward control.

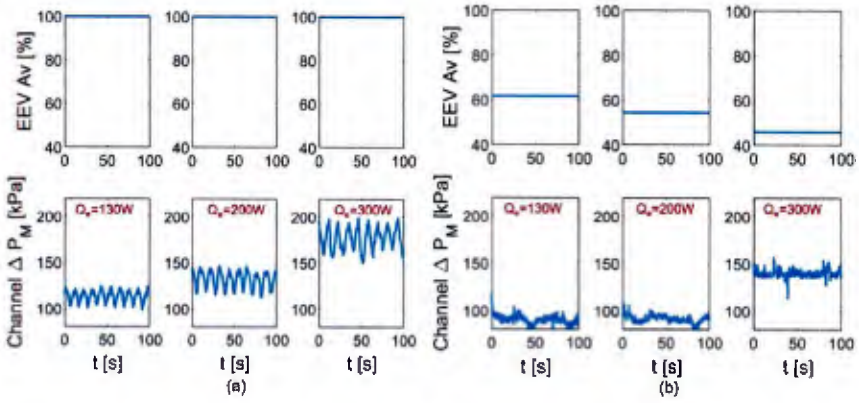

Figure 15: (a) System response without control; (b) System response with proportional valve control

5.2 Performance of a Pumped Liquid Cycle

Fig. 16(a) shows the pumped liquid cycle testbed used in this study. For simplicity, we tested an evaporator constructed using a stainless steel capillary tube with an internal diameter, $D = 1.5$ mm, and length, $L = 90$ mm. Fig. 16 (b) shows the pressure drop in the evaporator for different heat loads. In this case, a negative slope region was obtained, indicating the possibility of pressure drop oscillation at the system level. Fig. 16 (c) shows the heat transfer coefficient of the evaporator under different heat loads.

Computational modeling of the pumped liquid cycle, as conducted for the vapor compression cycle, indicates that several parameters, including the expansion valve setting, pump speed, and the evaporator heat load, can affect the characteristics of pressure drop oscillation. This was also demonstrated experimentally. For example, Fig. 17(a) shows how we altered system stability by changing the valve setting for a fixed evaporator heat load,

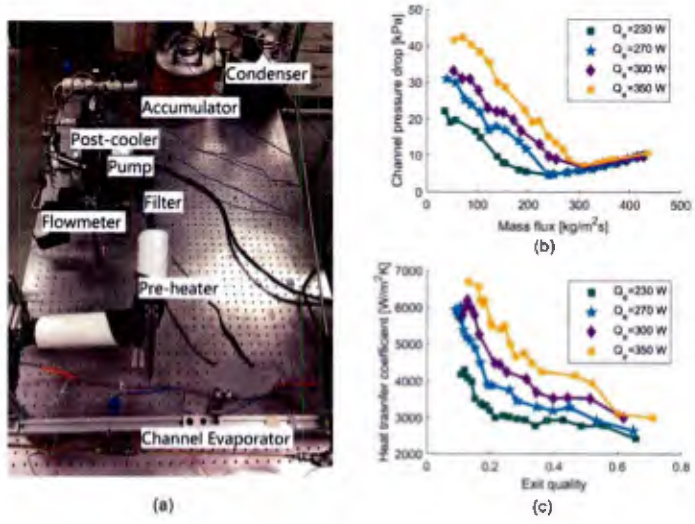

Figure 16: (a) Pumped liquid cycle test bed; (b) Channel pressure drop; (c) Heat transfer coefficient

Q_e = 300 W and pump speed, ω = 26 Hz, in the test-bed shown above. A smaller valve opening changes the demand pressure drop curve and thus stabilizes the system, which was also predicted by the computational model developed in this project. Similarly, the model also indicates that an increase in the evaporator heat load can affect the demand pressure drop, which can make the pressure drop oscillations more severe. Fig. 17(b) shows that the oscillations do become more severe with increasing evaporator heat load.

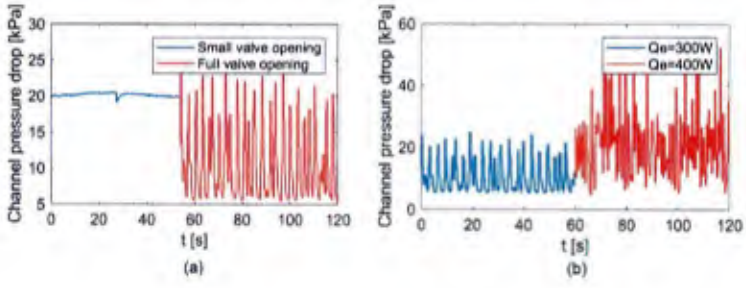

Figure 17: (a) Valve opening impact on oscillation at Q_e = 300 W, ω = 26 Hz; (b) Evaporator heat impact on oscillation at ω = 26 Hz, A_v = 100%

5.3 Comparison of Model Predictions and Experiments

Fig. 18 shows the experimental characterization of pressure drop in the pumped liquid cycle (Fig. 16) for single phase and two-phase flow. Also shown are the polynomial curves fitted to the experimental results for developing the lumped two-zone dynamic model. Solving the equations governing the system response, we compared the model predictions with experiments under different conditions. For example, Fig. 19 shows the comparison for an

evaporator heat load of $Q_e = 300$ W, indicating a good match. The experimentally validated model allows the design of a reliable control strategy to maintain safe operating conditions and avoid flow instability, as described earlier.

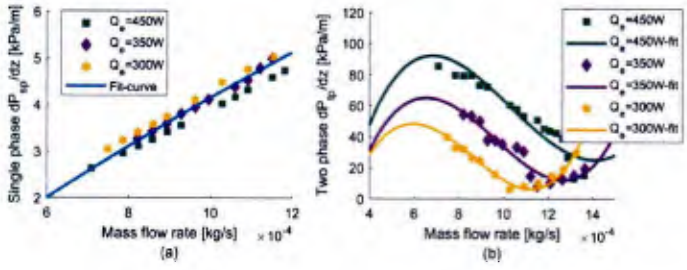

Figure 18: (a) Single-phase; (b) Two-phase pressure gradient fit

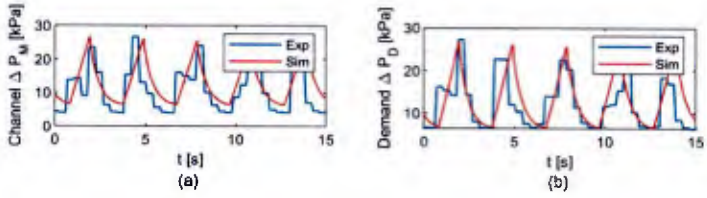

Figure 19: Experiment and simulation comparison (a) Channel pressure drop; (b) Demand pressure drop at $Q_e = 300$ W

6 Flow Maldistribution in Parallel Channels

Although microchannel evaporators are capable of removing large heat fluxes, flow maldistribution in the parallel channels of the evaporator can cause a considerable variation in the cooling performance of each channel. Such variations in performance are undesirable and present a significant challenge to implement this strategy effectively. In this project, we analyzed flow boiling in parallel channels to address the challenge posed by flow maldistribution.

6.1 Modeling Flow Maldistribution

For computational modeling of flow maldistribution, we considered a water-based two-phase system (Fig. 20) consisting of a partially-filled tank, a flow control valve, and two parallel channels [9, 27, 31, 32]. The model considers channels with a hydraulic diameter, $D = 1.5$ mm and length, $L = 85$ cm. Since the two channels have a common inlet and outlet, they are automatically flow-coupled. In other words, a pressure disturbance in one channel can affect the flow in the other channel. Analogous to flow-coupling, thermal-coupling can take place when the two channels can exchange heat. In this case, a temperature disturbance in one channel can affect the heat transfer in the other channel. For the two parallel channels

considered in this study, Fig. 21(a) shows the pressure drop, ΔP_M, as a function of flow rate and heat load, and Fig. 21(b) shows the heat transfer coefficient, H_e, as a function of exit quality and heat load.

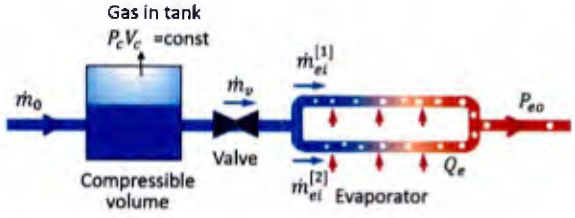

Figure 20: Schematic diagram of a two-channel evaporator system

The extent of flow coupling between the two channels is considered in the momentum balance as [33]:

$$\frac{d\dot{m}_e^{[i]}}{dt} = \frac{A_{cse}}{L_e}(P_{ei} - P_{eo} - \Delta P_M^{[i]} - U_p(\Delta P_M^{[j]} - \Delta P_M^{[i]})) \quad (1)$$

where $i,\ j = 1,\ 2$ and $i \neq j$. Here, $\dot{m}_e$ is the average flow rate, P_{ei} and P_{eo} are the inlet and outlet pressures, A_{cse} and L_e are the channel cross-section area and length, respectively. U_p is the coefficient denoting the extent of flow coupling between the channels, which depends on the flow conditions and the geometry of the channels.

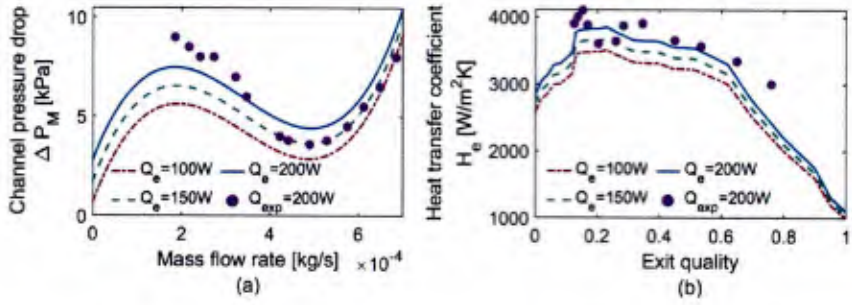

Figure 21: (a) Pressure drop in each channel as a function of mass flow rate and a given heat load, (b) Average heat transfer coefficient as a function of vapor quality at evaporator exit.

Similarly, by considering the thermal coupling between channels, the energy balance for the channel walls is given by [29,34]:

$$(\rho c_p V)_{we}\frac{dT_{we}^{[i]}}{dt} = Q_e^{[i]} - H_e^{[i]}A_{se}(T_{we}^{[i]} - T_{re}^{[i]}) + U_t\frac{k_{tc}A_{tc}}{t_{tc}}(T_{we}^{[j]} - T_{we}^{[i]}),\ i = 1,2; j = 2,1 \quad (2)$$

where Q_e is channel heat load. k_{tc} = 220 W/mK, t_{tc} = 1.5 mm and $A_{tc} = L_e \times D_h$ = 85 cm×1.5 mm are the thermal conductivity, wall thickness and area for interchannel heat transfer between thermally coupled channels, respectively. U_t is the coupling coefficient denoting the extent of thermal coupling between the channels, which also depends on the

channel geometry and flow conditions. The system performance can be predicted by solving the governing equations for different fluid and thermal coupling coefficients.

Fig. 22 shows the wall temperatures for the two channels ($T_{we}^{[1]}$, $T_{we}^{[2]}$) experiencing the same heat load of $Q_e^{[1]} = Q_e^{[2]} = 130$ W. In the presence of flow oscillations due to pressure drop instability, the lack of both flow and thermal coupling gives rise to a significant difference in the wall temperatures due to flow maldistribution. However, either flow or thermal coupling between the two channels allows them to perform equally well, resulting in a matching temperature response, as shown in Fig. 22(b) and (c). In summary, the computational model indicates that maldistribution effects in parallel channels can be mitigated if they are coupled strongly via heat transfer or fluid flow. We tested this hypothesis in experiments as well, as discussed below.

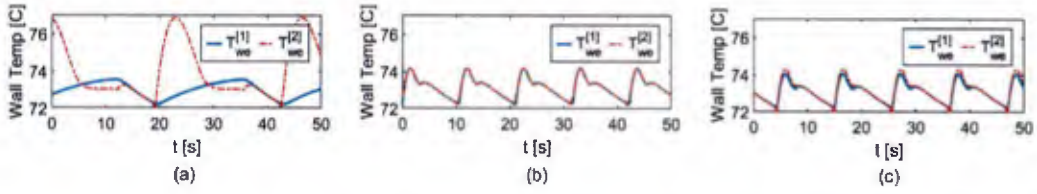

Figure 22: Temperature of the parallel channels with coupling coefficients as: (a) $U_t = 0$, $U_p = 0$; (b) $U_t = 44$, $U_p = 0$; (c) $U_t = 0$, $U_p = 0.3$.

6.2 Experimental Demonstration of Flow Synchronization

Fig. 23(a) shows the schematic diagram of the water-based pumped loop system used to study flow maldistribution. In this system, coolant (water) from the secondary condenser is pumped to a higher pressure, causing flow through the valve and the evaporator. As it enters the evaporator, the flow is split into two channels. The coolant absorbs heat as it flows across the channels, and exits as a liquid-vapor mixture. The fluid then enters the condenser, where it condenses by rejecting heat to the chiller, and then flows into the accumulator, which is maintained at a constant temperature. The system incorporates an evaporator with thermally-coupled channels constructed in an aluminum block with the following dimensions: Width $\times$ Depth $\times$ Length $=$ 1 mm $\times$ 0.5 mm $\times$ 100 mm. The wall between the channels is 4 mm thick. A single centrally-placed cartridge heater is used to provide heat to both channels, as illustrated in Fig. 23(b). A thermally-decoupled evaporator is also constructed using two stainless steel capillary tubes with the following dimensions: Diameter $\times$ Length $=$ 1.5 mm $\times$ 85 cm. In this case, rope heaters are used to heat the channels individually, as shown in Fig. 23(c).

6.3 Performance of Thermally-Coupled Channels

Fig. 24 shows the channel pressure drop and coolant outlet temperatures for thermally-coupled channels for different heat loads. Also shown is the saturation temperature, T_{sat} at the channel outlet, which is calculated based on the local pressure. The uncertainty in the pressure drop, saturation temperature, and outlet temperatures are indicated as ΔP_{Merr},

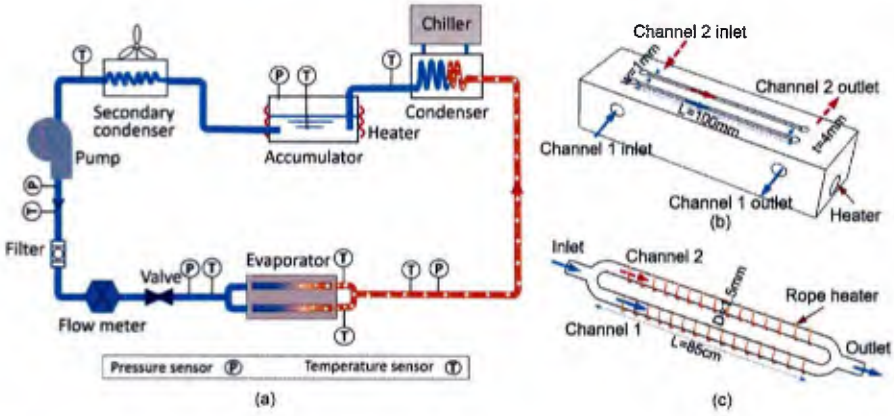

Figure 23: (a) Schematic diagram of the pumped loop system; (b) Evaporator design for thermally-coupled channels; (c) Evaporator design for thermally-decoupled channels

T_{saterr}, $T^{[1]}_{outerr}$ and $T^{[2]}_{outerr}$, respectively.

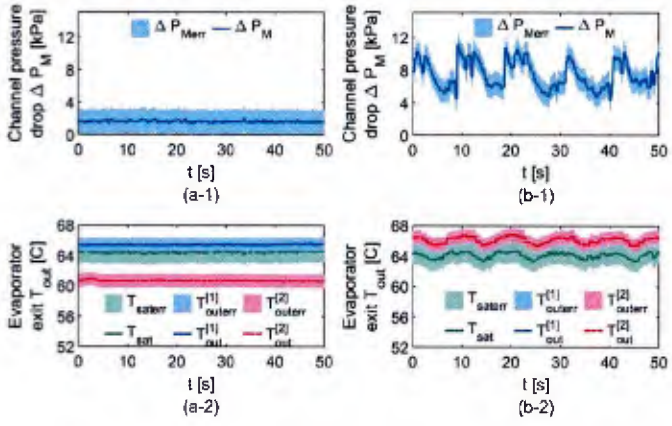

Figure 24: (a) Pressure drop (a-1) and coolant outlet temperatures (a-2) for thermally-coupled channels when Q_{etol} = 110 W and ω =30 Hz; (b) Pressure drop (b-1) and coolant outlet temperatures (b-2) for thermally-coupled channels when Q_{etot} = 175 W and ω =30 Hz.

When the channels receive a small heat load ($Q_e^{[1]} + Q_e^{[2]}$ = 110 W), the system is stable. Consequently, there are no oscillations in the channel pressure drop and temperature (Fig. 24(a-1) and (a-2)). However, spatial non-uniformity in temperature can still pose challenges, like the risk of dryout, due to flow maldistribution. In this case, the outlet temperatures indicate that the flow in one of the channels is two-phase while the other is single phase (Fig. 24(a-2)). With stable operating conditions, the difference in temperature can become much larger for higher heat loads or lower flow rates, which is clearly undesirable for cooling applications that require temperature uniformity. On the other hand, as predicted by the computational model, flow oscillations in the presence of thermal and flow coupling

can cause temperature synchronization. Experimentally, this takes place when the evaporator heat load is large enough (Q_{etot} = 175 W) to cause pressure drop instability resulting in flow oscillations, as shown in Fig. 24 (b-1) and (b-2). Flow oscillations cause the channel pressure drop to vary between 5 kPa and 12 kPa. While the channel outlet temperatures oscillate with an amplitude of 0.5 °C, they are well synchronized.

6.4 Performance of Thermally-Decoupled Channels

Fig. 25 shows the channel pressure drop, saturation temperature and coolant outlet temperatures for thermally-decoupled channels (Fig. 23(c)) for different evaporator heat loads. Also shown are the corresponding uncertainties in the pressure drop (ΔP_{Merr}), saturation temperature (T_{saterr}), and outlet temperatures ($T^{[1]}_{outerr}$ and $T^{[2]}_{outerr}$).

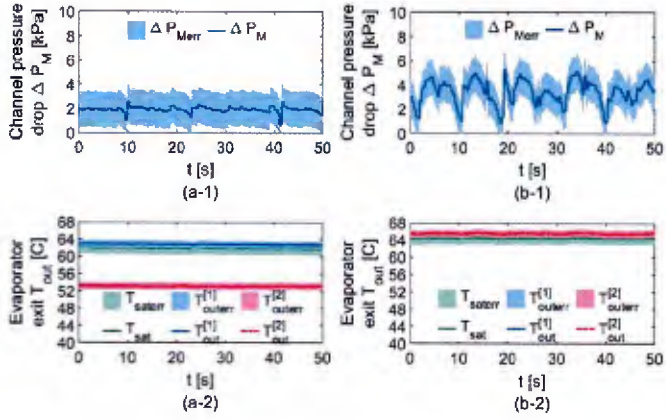

Figure 25: (a) Pressure drop (a-1) and coolant outlet temperatures (a-2) for thermally-decoupled channels for $Q_e^{[1]} = Q_e^{[2]}$ =70 W and ω =40Hz; (b) Pressure drop (b-1) and coolant outlet temperatures (b-2) for thermally-decoupled channels for $Q_e^{[1]} = Q_e^{[2]}$ =130 W and ω =40Hz

When the channel experiences a smaller heat load ($Q_e^{[1]} = Q_e^{[2]}$ = 70 W), the system is stable. As a result, there are no oscillations in the channel pressure drop and the outlet temperatures (Fig. 25(a-1), (a-2)). However, outlet temperatures of the fluid streams show a significant difference. An increase in the channel heat load ($Q_e^{[1]} = Q_e^{[2]}$ =130 W) causes pressure drop instability, which results in oscillations, as shown in Fig. 25(b-1) and (b-2). In this case, even in the absence of thermal coupling between the channels, the outlet temperatures of two fluid streams are synchronized due to a strong flow-coupling, as shown in Figs. 25.

The models and experiments indicate that the parallel channels of an evaporator can perform equally well if they can be coupled together by flow or heat transfer or both. The presence of flow oscillations seems to strengthen the flow coupling between the channels, and high thermal conductance between the channels can improve thermal-coupling to further mitigate the challenge posed by flow maldistribution. The flow and thermal coupling can be improved with careful selection of microchannel geometry and material to construct the

evaporator. Furthermore, artificially introduced flow oscillations could also mitigate the effects of flow maldistribution.

References

[1] S. V. Garimella, A. S. Fleischer, and J. Y. Murthy, "Thermal challenges in next-generation electronic systems," *IEEE Transactions on Components and Packaging Technologies*, vol. 31, no. 4, pp. 801–815, 2008.

[2] M. Ledinegg, "Instability of flow during natural and forced circulation," *Die Warme*, vol. 48, pp. 891–898, 1938.

[3] A. Stenning, "Instabilities in the flow of a boiling liquid," *Journal of Basic Engineering*, vol. 86, no. 2, pp. 213–217, 1964, DOI:10.1115/1.3653038.

[4] J. Lee and I. Mudawar, "Two-phase flow in high-heat-flux micro-channel heat sink for refrigeration cooling applications: Part ii—heat transfer characteristics," *International Journal of Heat and Mass Transfer*, vol. 48, no. 5, pp. 941–955, 2005, DOI:10.1016/j.ijheatmasstransfer.2004.09.019.

[5] S.-M. Kim and I. Mudawar, "Thermal design and operational limits of two-phase micro-channel heat sinks," *International Journal of Heat and Mass Transfer*, vol. 106, pp. 861–876, Mar. 2017, DOI:10.1016/j.ijheatmasstransfer.2016.10.020.

[6] J. Boure, A. Bergles, and L. Tong, "Review of two-phase flow instability," *Nuclear Engineering and Design*, vol. 25, no. 2, pp. 165–192, 1973.

[7] A. E. Bergles, J. H. Lienhard V, G. E. Kendall, and P. Griffith, "Boiling and evaporation in small diameter channels," *Heat Transfer Engineering*, vol. 24, no. 1, pp. 18–40, 2003, DOI:10.1080/01457630304041.

[8] T. Tong, T. Zhang, J. Chang, Y. Peles, R. Prasher, M. Jensen, J. Wen, and P. Phelan, "Ledinegg instability in microchannels," *International Journal of Heat and Mass Transfer*, vol. 52, no. 25, pp. 5661–5674, 2009, DOI:10.1016/j.ijheatmasstransfer.2009.09.008.

[9] T. Zhang, Y. Peles, J. T. Wen, T. Tong, J.-Y. Chang, R. Prasher, and M. K. Jensen, "Analysis and active control of pressure-drop flow instabilities in boiling microchannel systems," *International Journal of Heat and Mass Transfer*, vol. 53, no. 11, pp. 2347–2360, 2010, DOI:10.1016/j.ijheatmasstransfer.2010.02.005.

[10] S. Kakac and B. Bon, "A review of two-phase flow dynamic instabilities in tube boiling systems," *International Journal of Heat and Mass Transfer*, vol. 51, no. 3, pp. 399–433, 2008, DOI:10.1016/j.ijheatmasstransfer.2007.09.026.

[11] G. Patankar and T. R. Salamon, "Maldistribution of two-phase flow in parallel channel heat sinks: Effects of thermal connection between channels," in *2018 17th IEEE Intersociety Conference on Thermal and Thermomechanical Phenomena in Electronic Systems (ITherm)*. IEEE, 2018, pp. 653–663.

[12] G. Wang, P. Cheng, and A. Bergles, "Effects of inlet/outlet configurations on flow boiling instability in parallel microchannels," *International Journal of Heat and Mass Transfer*, vol. 51, no. 9-10, pp. 2267–2281, 2008, DOI: 10.1016/j.ijheatmasstransfer.2007.08.027.

[13] A. Koşar, C.-J. Kuo, and Y. Peles, "Boiling heat transfer in rectangular microchannels with reentrant cavities," *International Journal of Heat and Mass Transfer*, vol. 48, no. 23-24, pp. 4867–4886, 2005, DOI:10.1016/j.ijheatmasstransfer.2005.06.003.

[14] W. Qu and I. Mudawar, "Measurement and prediction of pressure drop in two-phase micro-channel heat sinks," *International Journal of Heat and Mass Transfer*, vol. 46, no. 15, pp. 2737–2753, 2003.

[15] H. J. Lee, D. Y. Liu, and S.-c. Yao, "Flow instability of evaporative micro-channels," *International Journal of Heat and Mass Transfer*, vol. 53, no. 9-10, pp. 1740–1749, 2010, DOI:10.1016/j.ijheatmasstransfer.2010.01.016.

[16] S. Szczukiewicz, N. Borhani, and J. R. Thome, "Two-phase flow operational maps for multi-microchannel evaporators," *International Journal of Heat and Fluid Flow*, vol. 42, pp. 176–189, 2013.

[17] T. Zhang, J. T. Wen, A. Julius, Y. Peles, and M. K. Jensen, "Stability analysis and maldistribution control of two-phase flow in parallel evaporating channels," *International Journal of Heat and Mass Transfer*, vol. 54, no. 25-26, pp. 5298–5305, 2011.

[18] S. G. Kandlikar, "High flux heat removal with microchannels — a roadmap of challenges and opportunities," *Heat Transfer Engineering*, vol. 26, no. 8, pp. 5–14, 2005, DOI:10.1080/01457630591003655.

[19] J. Lee and I. Mudawar, "Low-temperature two-phase microchannel cooling for high-heat-flux thermal management of defense electronics," *IEEE Transactions on components and packaging technologies*, vol. 32, no. 2, pp. 453–465, 2009.

[20] Q. Jin, J. T. Wen, and S. Narayanan, "Characteristics of pressure drop oscillation in a microchannel cooling system," *Applied Thermal Engineering*, p. 113849, 2019.

[21] ——, "The analysis and prediction of pressure drop oscillation in phase-change cooling systems," *International Journal of Heat and Mass Transfer*, vol. 165, Feb. 2021.

[22] ——, "Dynamic control of pressure drop oscillation in a microchannel cooling system," *Heat Transfer Engineering*, Jan. 2020.

[23] ——, "Temperature synchronization in microchannel cooling systems," *International Journal of Thermal Sciences*, vol. 156, Oct. 2020.

[24] ——, "Moving boundary model for dynamic control of multi-evaporator cooling systems facing variable heat loads," *International Journal on Refrigeration*, vol. 120, pp. 481–492, Dec. 2020.

[25] ——, "Dynamic control of microchannel cooling system with unanticipated evaporator heat loads," *Applied Thermal Engineering*, vol. 183, Jan. 2021.

[26] A. Koşar and Y. Peles, "Convective flow of refrigerant (r-123) across a bank of micro pin fins," *International Journal of Heat and Mass Transfer*, vol. 49, no. 17, pp. 3142–3155, 2006.

[27] L. Cao, S. Kakac, H. Liu, and P. Sarma, "Theoretical analysis of pressure-drop type instabilities in an upflow boiling system with an exit restriction," *Heat and Mass Transfer*, vol. 37, no. 4, pp. 475–483, 2001, DOI:10.1007/s002310000147.

[28] S. Saitoh, H. Daiguji, and E. Hihara, "Effect of tube diameter on boiling heat transfer of r-134a in horizontal small-diameter tubes," *International Journal of Heat and Mass Transfer*, vol. 48, no. 23, pp. 4973–4984, 2005, DOI:10.1016/j.ijheatmasstransfer.2005.03.035.

[29] D. Pollock, "Control-oriented dynamic modeling of vapor compression cycles for electronics cooling," *MS Thesis, Dept. Mech. Eng., Rensselaer Polytechnic Inst*, 2012, DOI:10.1115/1.1648312.

[30] Z. Yang, "Advanced control of vapor compression cycle for large and transient heat flux removal," Ph.D. dissertation, Rensselaer Polytechnic Institute, 2016.

[31] H. J. Lee and S. Y. Lee, "Heat transfer correlation for boiling flows in small rectangular horizontal channels with low aspect ratios," *International Journal of Multiphase Flow*, vol. 27, no. 12, pp. 2043–2062, 2001.

[32] S. Kakaç, M. R. Venkataraman, A. Pramuanjaroenkij, and I. Kotcioglu, "Modeling of two-phase flow instabilities in convective in-tube boiling horizontal systems," *J. of Thermal Science and Technology*, vol. 29, no. 1, pp. 107–116, 2009.

[33] H. Grzybowski and R. Mosdorf, "Modelling of pressure-drop instability in single and multi microchannels system," *acta mechanica et automatica*, vol. 6, no. 3, pp. 45–51, 2012.

[34] Q. Jin, J. T. Wen, and S. Narayanan, "Analysis and active control of pressure drop oscillation in microchannel vapor compression cycle," in *2018 17th Intersociety Conference on Thermal and Thermomechanical Phenomena in Electronic Systems*. IEEE, 29 May-1 June, San Diego, CA, USA, 2018, DOI:10.1109/ITHERM.2018.8419637, pp. 842–849.

Training

The following students have been supported on this project:

- Zehao Yang, Ph.D. in Mechanical, Aerospace, and Nuclear Engineering, Rensselaer Polytechnic Institute, completed in December 2016.

- Qi Jin, Ph.D. in Mechanical, Aerospace, and Nuclear Engineering, Rensselaer Polytechnic Institute, completed in December 2019.
- Toochukwu Aka, Ph.D. student in Mechanical, Aerospace, and Nuclear Engineering, Rensselaer Polytechnic Institute.
- Chalres Okaeme, Post-doctoral Research Associate in Mechanical, Aerospace, and Nuclear Engineering, Rensselaer Polytechnic Institute.
- Melissa Anne Shuey, Undergraduate Research Assistant, in Mechanical, Aerospace, and Nuclear Engineering, Rensselaer Polytechnic Institute.
- Kathleen Zheng, Undergraduate Research Assistant, in Mechanical, Aerospace, and Nuclear Engineering, Rensselaer Polytechnic Institute
- Qianqian Che, Undergraduate Research Assistant, in Electrical, Computer, and Systems Engineering, Rensselaer Polytechnic Institute

Dissemination

Journal Articles

Published

1. Q. Jin, J.T. Wen, S. Narayanan, "Characteristics of pressure drop oscillation in a microchannel cooling system," Applied Thermal Engineering, Vol. 160, 2019, 113849.
2. Q. Jin, J.T. Wen, S. Narayanan, "Dynamic control of pressure drop oscillation in a microchannel cooling system," Heat Transfer Engineering, Jan, 2020.
   DOI: 10.1080/01457632.2019.1707391.
3. Q. Jin , J.T. Wen, S. Narayanan, "Temperature Synchronization in Microchannel Cooling Systems," International Journal of Thermal Sciences. Vol. 156, October, 2020.
   DOI: 10.1016/j.ijthermalsci.2020.106476.
4. Q. Jin, J.T. Wen, S. Narayanan, "Moving boundary model for dynamic control of multi-evaporator cooling systems facing variable heat loads," International Journal on Refrigeration, Vol. 120, December, 2020, pp. 481-492.
5. Q. Jin, S. Narayanan, J.T. Wen, "Dynamic Control of Microchannel Cooling System with Unanticipated Evaporator Heat Loads," Applied Thermal Engineering, Vol. 183, Part 2, Jan, 2021.
   DOI: 10.1016/j.applthermaleng.2020.116225.
6. Q. Jin, J.T. Wen, S. Narayanan, "The Analysis and Prediction of Pressure Drop Oscillation in Phase-change Cooling Systems," International Journal of Heat and Mass Transfer, Vol. 165, Feb. 2021.
   DOI: 10.1016/j.ijheatmasstransfer.2020.120621

Conference Articles

- Q. Jin, J.T. Wen, S. Narayanan, "Characteristics of pressure drop instability in microchannel cooling system," 6th Micro and Nano Flows (MNF) Conference, Atlanta, GA, Sep, 2018.
- Q. Jin, J.T. Wen, S. Narayanan, "Analysis and active control of pressure drop oscillation in microchannel vapor compression cycle," The Intersociety Conference on Thermal and Thermomechanical Phenomena in Electronic Systems, San Diego, CA, May 29-Jun. 1, 2018.

Conference Presentations

1. Q. Jin, J.T. Wen, S. Narayanan, "Moving boundary model for dynamic control of two microchannel evaporator cooling system," International Technical Conference and Exhibition on Packaging and Integration of Electronic and Photonic Microsystems, Oct 7-9, Anaheim, CA, 2019.
2. J.T. Wen, "Active Transient Control of Two-Phase Cooling Systems," in Itherm Invited Session on Thermal Management in the Aerospace, Automotive and Telecommunications Industries, Las Vegas, NV, May 29, 2019
3. Q. Jin, J.T. Wen, S. Narayanan, "Control of microchannel cooling system under transient heat load," New York Manufacturing Conference, May 1, Troy, NY, 2019.
4. Q. Jin, J.T. Wen, S. Narayanan, "Characteristics of pressure drop instability in microchannel cooling system," 6th Micro and Nano Flows Conference, Atlanta, GA, USA, September 9-12, 2018.
5. Q. Jin, J.T. Wen, S. Narayanan, "Analysis and active control of pressure drop oscillation in microchannel vapor compression cycle," The Intersociety Conference on Thermal and Thermomechanical Phenomena in Electronic Systems, San Diego, CA, May 29 - June 1, 2018.

Honors

Shankar Narayanan:

- NSF CAREER Award: "Using High-resolution Piezoelectric Sensing to Investigate Liquid-vapor Phase-change Mechanisms in Nanostructures"
- NASA Young Investigator Award: "Three-dimensional Hierarchical Structures as Multilayer Insulation for Terrestrial and Space Applications"
- ACS PRF Doctoral New Investigator Award: "Separation of Oil-Water Emulsions using Nanoengineered Surfaces"

Technology Transfer

None

Participants

- John Wen: Co-Principal Investigator
- Shankar Narayanan: Co-Principal Investigator
- Qi Jin: Ph.D. Student
- Toochukwu Aka: Ph.D. Student
- Zehao Yang: Ph.D. Student
- Agung Julius: Faculty Participant
- Chalres Okaeme, Post-doctoral Research Associate
- Melissa Anne Shuey, Undergraduate Research Assistant
- Kathleen Zheng, Undergraduate Research Assistant
- Qianqian Che, Undergraduate Research Assistant